A&A, 707, L15 (2026)
https://doi.org/10.1051/0004-6361/202558825


Astronomy & Astrophysics

LETTER TO THE EDITOR

# Unclustered tracers remain unclustered

## The lack of primordial non-Gaussianity response of bias-zero tracers

C. Merino[1], S. Avila[1,⋆], A. G. Adame[2,3], A. Anguren[2], V. Gonzalez-Perez[2,4], and J. Meneses-Rizo[5]

[1] Centro de Investigaciones Energéticas, Medioambientales y Tecnológicas (CIEMAT), Madrid, Spain
[2] Departamento de Física Teórica, Universidad Autónoma de Madrid, 28049 Madrid, Spain
[3] Department of Astrophysics, University of Vienna, Türkenschanzstrasse 17, 1180 Vienna, Austria
[4] Centro de Investigación Avanzada en Física Fundamental (CIAFF), Universidad Autónoma de Madrid, ES-28049 Madrid, Spain
[5] Instituto de Física, Universidad Nacional Autónoma de México, Apdo. Postal 20-364 Ciudad de México, Mexico

Received 30 December 2025 / Accepted 14 February 2026

**ABSTRACT**

Constraining primordial non-Gaussianities (PNGs) is one of the main goals of new-generation large-scale galaxy surveys. It had been proposed that unclustered tracers (with bias $b_1 = 0$) could be optimal for PNG studies, and that these could be found by selecting galaxies in bins of their local density. We tested this hypothesis in state-of-the-art simulations from the PNG-UNITsim suite with local $f_{\rm NL} = 100$ and $f_{\rm NL} = -20$. We considered different parent tracer catalogues: all haloes together, haloes in broad mass bins, and halo occupation distribution (HOD) models for luminous red galaxies (LRGs) and quasars (QSOs). We then classify these tracers by their local density ($\delta_{t,R}$) and measure the linear bias ($b_1$) and PNG response ($b_\phi$). Most $\delta_{t,R}$ bins show a PNG response compatible with $b_\phi = 0$ for all haloes or the low-mass bin ($\log M < 11$). For high-mass haloes ($\log M > 12$), QSO or LRG, we recover a trend closer to the universality relation ($b_\phi = 2\delta_{\rm crit}(b_1 - 1)$) for $b_1 > 1$, but the $b_\phi(b_1)$ curve flattens to 0 below $|b_1| < 1$. Hence, we find $b_\phi \approx 0$ for all bias-zero tracers considered. The complex $\delta_{t,R}$-based selection causes their clustering to strongly deviate from simple assumptions, namely the universality relation and Poisson shot noise, hindering their capability to constrain PNGs.

**Key words.** early Universe – large-scale structure of Universe – inflation

## 1. Introduction

Cosmic inflation–a phase of accelerated expansion during the first moments of the Universe–was postulated as a solution to some of the problems of the Hot Big Bang theory associated with the initial conditions (ICs; Guth 1981; Linde 1982). It also explains the origin of the inhomogeneities giving rise to the large-scale structure of the Universe (LSS). Although inflation is assumed to be part of the standard model in most modern cosmological analyses, the exact physics driving it remains unknown, as a wide variety of physical models can produce inflation.

One observable that discriminates among families of models is primordial non-Gaussianity (PNG). We focus on the simplest PNG, local-$f_{\rm NL}$ (Komatsu & Spergel 2001), which introduces quadratic expansion of a Gaussian gravitational field, $\phi_G$,

$$\phi(\mathbf{x}) = \phi_G(\mathbf{x}) + f_{\rm NL}\left(\phi_G(\mathbf{x})^2 - \langle\phi_G(\mathbf{x})^2\rangle\right), \tag{1}$$

where $\langle\cdot\rangle$ represents a spatial average. Typically, this parameter is predicted to be $f_{\rm NL} > O(1)$ for inflation driven by multiple fields (Byrnes & Choi 2010; Alvarez et al. 2014).

Although the primary effect of local-$f_{\rm NL}$ is to generate a primordial bispectrum, the non-linear evolution of the LSS allows us to study PNG through two-point statistics. Galaxies ($g$) or haloes ($h$) are biased tracers ($t$) of the matter ($m$) density. At large scales, this is given by a linear relation of overdensity ($\delta$):

$$\delta_t = b \cdot \delta_m. \tag{2}$$

For Gaussian initial conditions, the large-scale bias is simply a constant, $b_1$, the linear bias. However, when including PNG, the bias becomes scale-dependent (Dalal et al. 2008; Slosar et al. 2008; Matarrese & Verde 2008):

$$b(k,z) = b_1(z) + \frac{f_{\rm NL} b_\phi(z)}{\alpha(k,z)}. \tag{3}$$

Here $b_\phi$ is a bias parameter associated with the gravitational field, $\phi$, related to the overdensity field via

$$\delta(k,z) = \alpha(k,z)\,\phi(k,z), \quad \text{with} \quad \alpha(k,z) = k^2\,T(k)\cdot\frac{2}{3}\frac{D(z)}{\Omega_M}\frac{c^2}{H_0^2}, \tag{4}$$

where $D(z)$ is the growth factor normalised to $(1+z)^{-1}$ in the radiation era, $T(k)$ is the transfer function (with $T(k\to 0)\to 1$), $\Omega_M$ is the current matter density, $H_0$ the Hubble constant, and $c$ the speed of light. The PNG universality relation is given by (Dalal et al. 2008)

$$b_\phi = 2\delta_{\rm crit}(b_1 - p) \quad \text{with} \quad p = 1, \tag{5}$$

where $\delta_{\rm crit}$ is the critical density for spherical collapse (1.686).

Many galaxy surveys, such as DESI, Euclid, or SPHEREx, aim to constrain $f_{\rm NL}$ with Eq. (3). Identifying observables that

⋆ Corresponding author: santiagoj.avila@ciemat.es

maximise the PNG signal would be highly valuable in order to better understand inflation. In that context, Castorina et al. (2018) postulated that unclustered ($b_1 = 0$) tracers would be optimal in a regime with negligible shot noise ($P_{\rm shot}$), with an error given by

$$\sigma(f_{\rm NL})^{-2} \propto \frac{b_1^2 b_\phi^2}{\left(b_1^2 P_{mm}(k) + P_{\rm shot}\right)^2}, \tag{6}$$

with $P_{mm}(k)$ the matter power spectrum.

The way to find bias-zero tracers proposed in that work is by binning tracers according to their local density. They showed that unclustered tracers can be found in dark matter halo catalogues from cosmological $N$-body simulations with Gaussian ICs.

The goal of this letter is to verify or disprove the feasibility of using bias-zero tracers selected by local overdensity to set strong constraints on PNGs. For that, we use state-of-the-art $N$-body simulations with PNGs from the PNG-UNITsim suites (Adame et al. 2024).

## 2. Simulations

The PNG-UNIT simulation is an $N$-Body simulation (Adame et al. 2024), which is a twin of one of the UNITsims (Chuang et al. 2019), with the same size ($L = 1\,h^{-1}$ Gpc) and resolution ($N_{\rm part} = 4096^3$, $m_p = 1.2 \times 10^9\,h^{-1}\,M_\odot$), and that uses the same white noise for the ICs and ΛCDM parameters (based on Planck Collaboration XIII 2016); the only difference is the inclusion of a PNG of local-$f_{\rm NL} = 100$. This makes it one of the PNG simulations with the highest mass resolution and one of the largest in terms of particles. For this work we used the $z = 1$ ROCKSTAR (Behroozi et al. 2013) halo catalogues. These simulations are publicly available[1].

The PNG-UNITsim-XL we used here is a $L = 3\,h^{-1}$ Gpc simulation with $N = 4096^3$ particles and initial conditions with $f_{\rm NL} = -20$, which is a twin of a $f_{\rm NL} = 0$ UNITsim-XL simulation. These simulations are fully described in Adame et al. (in prep.). Both these simulations have been populated with a halo occupation distribution (HOD) model (Avila et al. 2020) matching the galaxy bias of DESI's Luminous Red Galaxies (LRG, using a snapshot at $z = 0.74$) and quasars (QSO, using $z = 1.83$). The HOD is first set to have a maximum of ∼1 for central galaxies and is later downsampled (by a factor of ∼2 and ∼40 for LRGs and QSOs, respectively) to match the number density of DESI. In this work we show the results for the full density samples, while we checked that results are consistent, but noisier, for the realistic-density sample.

## 3. Methodology

The potential of bias-zero tracers is illustrated in Fig. 1: an unclustered tracer in a Gaussian universe ($b_1 = 0$, black line) would cluster in PNG universes (green line) with a $1/k^2$ pattern. In this section we describe the methodology to test that.

### 3.1. Density classification

Unclustered tracers are expected to be found in regions that are neither very dense nor very empty. We follow the approach of Castorina et al. (2018) and classify tracers according to their density in spheres of radius $R$, $\delta_{t,R}$, using by default

[1] https://opendata.pic.es/unitsims

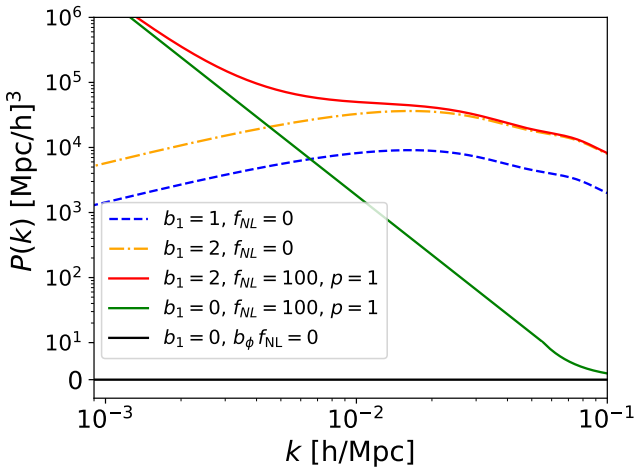


**Fig. 1.** Theoretical auto-power spectra for matter ($b = 1$, $f_{\rm NL} = 0$), a biased tracer in a Gaussian Universe ($b_g = 2$, $f_{\rm NL} = 0$), a biased universal tracer with PNG ($b_g = 2$, $f_{\rm NL} = 100$, $p = 1$), an unclustered but universal tracer ($b_g = 0$, $f_{\rm NL} = 100$, $p = 1$), and an unclustered and non-PNG-responsive tracer ($b_g = 0$, $b_\phi = 0$).

$R = 8\,h^{-1}$ Mpc. For this purpose, we use the SCIPY function CKDTREE. We considered different options for the parent samples:

- All haloes in the PNG-UNITsims above 20 particles;
- PNG-UNItsim haloes split into three mass bins: $10.5 < \log M < 11$, $11 < \log M < 12$, and $\log M > 12$;
- LRGs and QSOs from a HOD applied to PNG-UNITsim-XL.

For this paper we focused on equal-number $\delta_{t,R}$ bins, starting from the parent catalogues. We used 20 bins for haloes and 10 bins for galaxies. For better comparison with Castorina et al. (2018), we also reproduced their method based on only splitting the parent sample into two local density subsamples. We then kept the lower one: $\delta_{t,R} < \delta_{t,R}^{\rm max}$. As we vary the parameter $\delta_{t,R}^{\rm max}$, we measure the linear bias of the sample, until we find $b_1 \approx 0$.

### 3.2. Parameter fitting

For each subsample of interest, we compute the tracer auto-power spectrum $P_{tt}(k)$ and the tracer-matter cross-power spectrum $P_{tm}(k)$ with NBODYKIT (Hand et al. 2018). We additionally compute the matter power spectrum $P_{mm}(k)$, so that we can estimate the bias parameters by fitting the equations

$$\begin{aligned} P_{tm}(k) &= \left(b_1 + f_{\rm NL}\, b_\phi\, \alpha(k)^{-1}\right) P_{mm}(k), \\ P_{tt}(k) &= \left(b_1 + f_{\rm NL}\, b_\phi\, \alpha(k)^{-1}\right)^2 P_{mm}(k) + \tfrac{A_{\rm sn}}{n}, \end{aligned} \tag{7}$$

where we fit the free parameters $b_1$, $b_\phi$, and $A_{\rm sn}$. Here $A_{\rm sn}$ represents the shot noise deviation from the Poisson prediction $(1/n)$.

We use a Gaussian diagonal covariance (Smith 2009)

$$\begin{aligned} \sigma_{tt}(k)^2 &= \left(P_{tt}(k) + \tfrac{A_{sn}}{n}\right)^2 \cdot \tfrac{2\,(2\pi)^3}{4\pi\, k^2 \Delta k\, V} \quad \text{and} \\ \sigma_{tm}(k)^2 &= \left[\left(P_{tt}(k) + \tfrac{A_{sn}}{n}\right) P_{mm}(k) + P_{tm}(k)^2\right] \tfrac{(2\pi)^3}{4\pi\, k^2 \Delta k\, V}, \end{aligned} \tag{8}$$

where $V = L^3$ is the volume and $\Delta k$ is the $k$-bin width, which we set to the size of the fundamental mode $k_f = 2\pi/L$.

We fit the parameters using a Markov chain Monte Carlo (MCMC) algorithm with the EMCEE library from the cross-power spectrum up to $k_{\rm max} = 0.08\,h\,{\rm Mpc}^{-1}$. We validate our methodology in Appendix A.

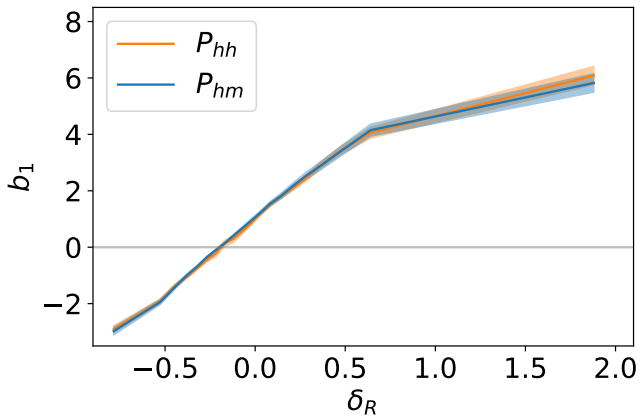


**Fig. 2.** Measured linear halo bias $b_1$ (68% c.l.) as a function of halo overdensity $\delta_{h,R}$ in spheres of $R = 8\,h^{-1}$ Mpc for the UNIT simulation ($f_{\rm NL} = 0$). Similar results are found for $f_{\rm NL} = 100$.

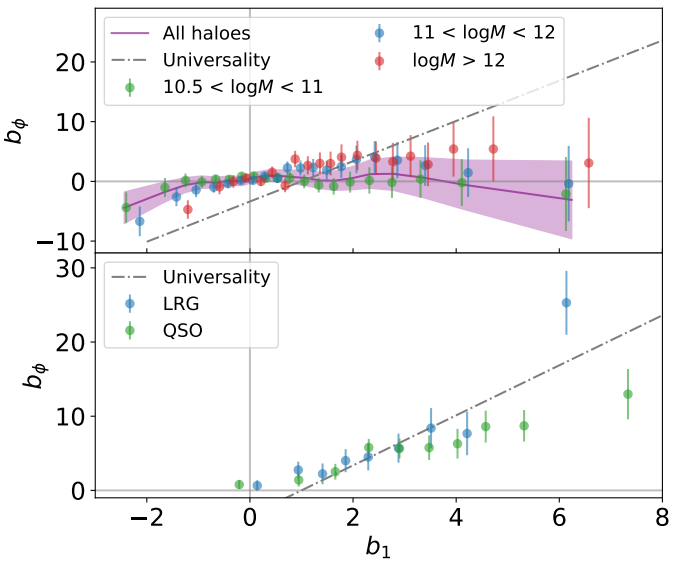


**Fig. 3.** PNG-response ($b_\phi$) as a function of the measured bias ($b_1$) for the tracers binned in their local overdensity. Top: Results for all haloes (purple band) together. The black dot-dashed line shows the universality relation. We find the PNG response well below the universality relation and compatible with no response ($b_\phi \sim 0$). We also show (as markers with errorbars) the results using mass bins as parent catalogues. Bottom: Same results, but for the LRGs and QSOs from PNG-UNITsim-XL.

## 4. Results

### 4.1. Halo density bins

The linear bias of haloes grows monotonically with their local density $\delta_{h,R}$. This is shown for the UNIT simulation ($f_{\rm NL} = 0$) haloes with at least 20 particles ($M_h > 2 \times 10^{10}$) in Fig. 2. For this measurement, we fit the linear bias ($b_1$) and shot-noise parameter ($A_{sn}$), while fixing $f_{\rm NL} = 0$. Figure 2 also shows the agreement between the results using the auto- and cross-power spectra. These results are in line with Castorina et al. (2018), and allow us to find the $b_1 \approx 0$ tracers.

For the PNG-UNIT simulation ($f_{\rm NL} = 100$) haloes, we additionally fit for $b_\phi$, while fixing $f_{\rm NL} = 100$. The $b_1(\delta_{h,R})$ relation measured from the cross-correlation is nearly identical to the $f_{\rm NL} = 0$ case. However, for the auto-correlation, the fits near $b_1 \approx 0$ are more numerically unstable, with $b_1$ absorbing the shot noise. For simplicity, we focus here on the cross-correlation results.

At linear scales, $\delta_h = b_1 \delta_M$. Hence, one would expect that we measure something compatible with $b_1 = 0$ whenever $\delta_h = 0$. However, this is not exactly what we see in Fig. 2, where the curve does not cross $\{b_1 = 0, \delta_{h,R} = 0\}$. This arises because $R = 8\,h^{-1}$ Mpc is mildly non-linear; we verified that increasing $R$ does not change our conclusions, while approaching the $\{b_1 = 0, \delta_{h,R} = 0\}$ crossing.

Another interesting feature is that the best fit for $A_{sn}$ typically ranges in 20−40, with $A_{sn} = 27$ for the bin closest to $b_1 = 0$. Castorina et al. (2018) already showed that these tracers were more stochastic than Poisson, but the factor found here is even higher, which might be due to the increased number density (and reduced baseline shot noise). This contribution of a factor of ∼30 in the increase in shot noise already suggests that using these tracers as optimal for PNG will be challenging, according to Eq. (6). We observe that $A_{sn}$ becomes higher for larger $R$, suggesting this effect comes from the exclusion of tracers.

We now move to the central idea of the paper using the PNG-UNITsim haloes with $f_{\rm NL} = 100$. In the top panel of Fig. 3 we represent the fitted $b_\phi$ against the linear bias for all haloes when classified in bins of $\delta_{t,R}$ as explained in Sect. 3.1.

We find that $b_\phi$ strongly deviates from the universality relation (Eq. (5)) marked by the dot-dashed line in Fig. 3. Moreover, we find that $b_\phi$ is compatible with zero for most of the $\delta_{h,R}$ bins. In particular, the bins close to $b_1 = 0$ are clearly vanishing.

### 4.2. Mass and halo density bins

A more realistic scenario is that you have a galaxy sample that is typically associated with a mass range. In Castorina et al. (2018), they test three mass bins as parent catalogues, similar to the three bins used here and defined in Sect. 3.1. We also show the $b_\phi(b_1)$ results for the mass bins in the top panel of Fig. 3. Remarkably, for the lower mass bin, we find a very flat $b_\phi(b_1) \sim 0$ curve (as in Sect. 4.1). On the other hand, the medium- and high-mass bins show a mild PNG response for $|b_1| > 1$, but are still typically below the universality relation. The excess of shot noise becomes more moderate for mass bins; in increasing order, we find $A_{\rm sn} = 13$, 7, and 2.

### 4.3. Galaxies in density bins

We now use a more realistic scenario, where we sample the halo catalogue with an HOD, representing DESI QSOs and LRGs in the PNG-UNITsim-XL simulations. While we show the results for the high-density samples (see Sect. 2), these are consistent with those from the realistic scenario, but less noisy.

The results are shown at the bottom of Fig. 3. In this case, the results follow a trend that is more similar to the universality relation. Nevertheless, the points near $b_1 = 0$ are still very compatible with $|b_\phi| = 0$ and clearly below the universality relation. In this case, the excess of shot noise is more moderated with $A_{sn} = 1.26$ for LRGs and $A_{sn} = 1.21$ for QSOs.

### 4.4. Density splits for all parent catalogues

Finally, we use an approach that is matched to the original Castorina et al. (2018) proposal: splitting each of the parent haloes in just two density bins, according to a $\delta_{r,R}^{\rm max}$. For each of the parent catalogues, we identify the $\delta_{t,R}^{\rm max}$ that makes $b_1$ closest to zero, and plot the values of $b_\phi$ for each of them in Fig. 4, and

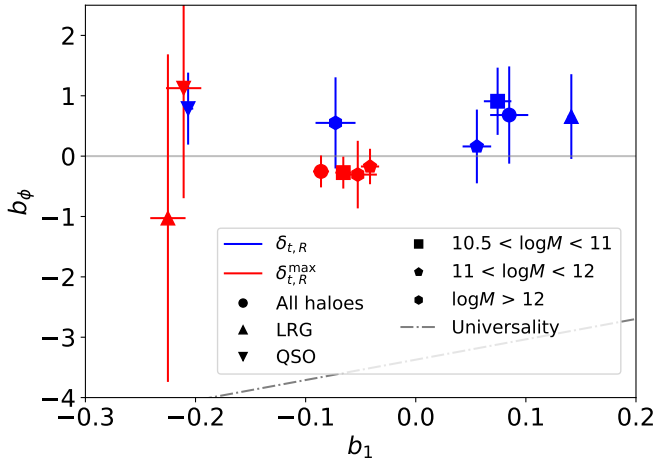


**Fig. 4.** PNG response ($b_\phi$) and linear bias ($b_1$) measurements for the closest case to $b_1 = 0$ for the density bins (blue) and density split (red) samples. We consider different parent catalogues: all haloes, haloes in mass bins, and HODs (Sect. 3.1). For all cases, the PNG response is clearly smaller than predicted by universality (dot-dashed line) and compatible with $b_\phi = 0$.

compare the results to the equivalent results from the $\delta_{t,R}$ bins. We find all of these cases to also be compatible with $b_\phi = 0$.

## 5. Discussion and conclusions

In this work we have used state-of-the-art PNG simulations from the PNG-UNITsim suite to evaluate the efficiency of unclustered tracers ($b_1 = 0$) for the study of local-PNGs as postulated by Castorina et al. (2018). We classified a parent tracer catalogue (all haloes, haloes in mass bins, or HOD-based galaxies) by their local density $\delta_{t,R}$ in spheres of $R = 8\,h^{-1}$ Mpc to measure their linear bias ($b_1$) and the PNG response ($b_\phi$) from the cross-power spectrum of the $\delta_{t,R}$-selected tracers and the matter field.

When considering all haloes at once or low-mass haloes ($10.5 < \log M < 11$), this method leads to $b_\phi(b_1) \approx 0$ for all $\delta_{t,R}$ bins (except below $b_1 \sim -1.5$). This implies that these tracers will remain unclustered after the inclusion of PNG. More graphically, they will follow the black line in Fig. 1 and not the green line. In the case of the medium-mass and higher mass bins ($11 < \log M < 12$, $\log M > 12$), we recover a slight hint for $b_\phi \neq 0$, but only for $|b_1| > 1$. When considering a parent sample of LRGs and QSOs from a HOD model, matching the galaxy bias of DESI, we recover a $b_\phi(b_1)$ curve closer to universality (Eq. (5)) for $b_1 > 1$, but that still flattens to $b_\phi = 0$ for $b_1 \approx 0$.

In summary, all unclustered tracers ($b_1 \sim 0$) found here remain unclustered with the inclusion of local-PNGs (Fig. 4), strongly deviating from the universality relation. In addition to the density bins, we also considered splitting the sample into two subsamples given a $\delta^{\max}_{t,R}$, and found qualitatively similar results. We also verified that the results mentioned above are robust to scale-cuts, the usage of auto- and cross-power spectra, and the variation in the smoothing scale $R$ (from 4 to 30 $h^{-1}$ Mpc). A similar trend is also found in Appendix B when classifying haloes in matter density instead of halo or galaxy density. We note that for $b_\phi = 0$ the Fisher information in $f_{\rm NL}$ (Eq. (6)) will vanish, leaving $f_{\rm NL}$ unconstrained. In addition, we find that these samples tend to have super-Poissonian shot noise, sometimes by a factor of ∼30, also complicating the optimality.

This $b_\phi(b_1 \approx 0) \approx 0$ relation reduces the effectiveness of constraining PNGs. As an example, if we do a Fisher forecast for the LRGs and QSOs modelled in PNG-UNITsim-XL for the DESI volume and number density, we obtain, respectively, $\sigma_{f_{\rm NL}} = 4.1$ and $\sigma_{f_{\rm NL}} = 3.8$. When considering their $\delta_{h,R}$ bin closest to $b_1 = 0$, even if neglecting shot noise, we obtain respectively, $\sigma_{f_{\rm NL}} = 133$ and $\sigma_{f_{\rm NL}} = 102$. Additionally, the $b_\phi(b_1 = 0) = 0$ relation would also hinder a multi-tracer analysis, where $\sigma(f_{\rm NL})^{-2} \propto |b_1^A b_\phi^B - b_1^B b_\phi^A|$ (Barreira & Krause 2023).

The lack of a PNG response appears in tension with the results reported by Castorina et al. (2018), where they found a PNG response of up to $b_\phi \approx 2.5$ for a $b_1 = 0$ tracer from their $\log M > 12.5$ parent catalogue[2]. This difference could possibly arise because that work used separate-universe simulations (with $f_{\rm NL} = 0$) to estimate $b_\phi$ as a derivative of the number of tracers with respect to the amplitude of primordial fluctuations ($A_s$). Whereas the separate-universe approach has been tested in halo mass bins (Biagetti et al. 2017), the selection based on the local halo density inherently brings higher order terms (in density and bias) to the selection that could in turn have cosmology dependence (including $A_s$). This possibility is supported by Morawetz et al. (2025) who found that $\delta_{h,R}$-selected tracers (from a parent catalogue of $\log M > 13.5$ haloes) have a PNG response that deviates from the separate-universe prediction (see their Fig. 9).

Exploring the PNG signal from alternative methods and samples is a powerful way to maximise the information from current and future missions. This work remarks on the importance of developing in parallel realistic suite of simulations to validate and improve the modelling of these less standard statistics.

*Acknowledgements.* We thank discussions with E. Paillas, J. L. Bernal, R. Angulo and I. Sevilla. SA has been funded by MCIN/AEI/10.13039/501100011033 and FSE+ (Europe) under project PID2024-156844NA-C22 and the RYC2022-037311-I fellowship. VGP is supported by the CNS2024-154242 grant. *Contributions:* CM led the analysis and figure making. SA led the conceptual design of the project and writing of the paper. AGA contributed to the analysis and interpretation. AA led a first version of the analysis. AGA, SA and VGP led the simulation construction. JMR constructed the HOD catalogues.

## References

Adame, A. G., Avila, S., Gonzalez-Perez, V., et al. 2024, A&A, 689, A69
Alvarez, M., Baldauf, T., Bond, J. R., et al. 2014, arXiv e-prints [arXiv:1412.4671]
Avila, S., Gonzalez-Perez, V., Mohammad, F. G., et al. 2020, MNRAS, 499, 5486
Barreira, A., & Krause, E. 2023, JCAP, 2023, 044
Behroozi, P. S., Wechsler, R. H., & Wu, H.-Y. 2013, ApJ, 762, 109
Biagetti, M., Lazeyras, T., Baldauf, T., Desjacques, V., & Schmidt, F. 2017, MNRAS, 468, 3277
Byrnes, C. T., & Choi, K.-Y. 2010, Adv. Astron., 2010, 1
Castorina, E., Feng, Y., Seljak, U., & Villaescusa-Navarro, F. 2018, Phys. Rev. Lett., 121, 101301
Chuang, C.-H., Yepes, G., Kitaura, F.-S., et al. 2019, MNRAS, 487, 48
Dalal, N., Doré, O., Huterer, D., & Shirokov, A. 2008, Phys. Rev., D, 77
Guth, A. H. 1981, Phys. Rev. D, 23, 347
Hand, N., Feng, Y., Beutler, F., et al. 2018, AJ, 156, 160
Komatsu, E., & Spergel, D. N. 2001, Phys. Rev. D, 63, 063002
Linde, A. D. 1982, Phys. Lett. B, 108, 389
Matarrese, S., & Verde, L. 2008, ApJ, 677, L77
Morawetz, J., Paillas, E., & Percival, W. J. 2025, JCAP, 2025, 026
Planck Collaboration XIII. 2016, A&A, 594, A13
Slosar, A., Hirata, C., Seljak, U., Ho, S., & Padmanabhan, N. 2008, JCAP, 2008, 031
Smith, R. E. 2009, MNRAS, 400, 851

[2] We verified our conclusions remain unchanged for $\log M > 12.5$.

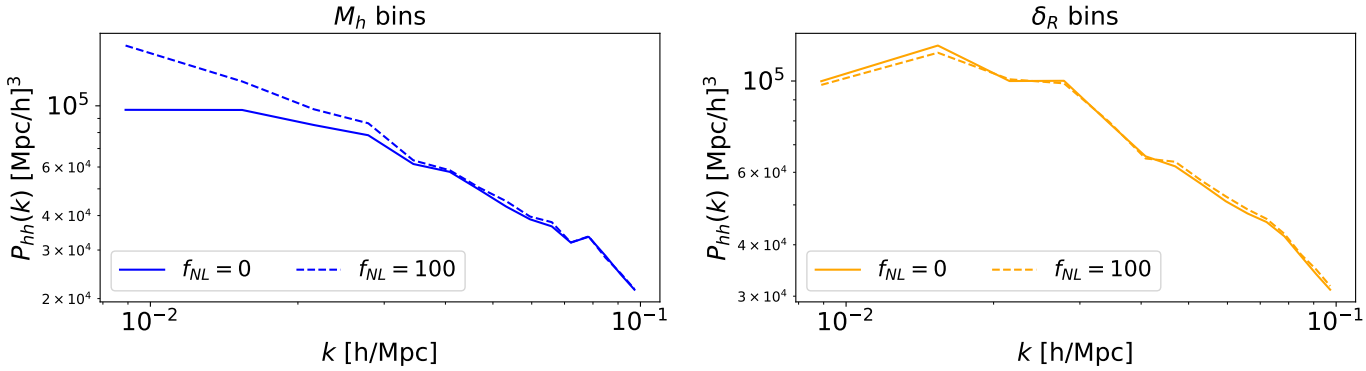


**Fig. A.1.** Power spectrum of a bin with $b_1 \sim 3.2$ selected by halo mass ($M_h$, **left**) and by local halo overdensity ($\delta_{h,R}$, **right**). Whereas the effect of introducing PNG ($f_{\rm NL} = 100$) has a strong effect on mass-selected bins, the $\delta_{h,R}$ bins show near identical clustering for $f_{\rm NL} = 0$ and $f_{\rm NL} = 100$.

## Appendix A: The lack of PNG signal

The flat curve for $b_\phi(b_1) = 0$ at the top of Fig. 3 can be somewhat surprising at first. To discard errors in the analysis, we verified that for simple halo-mass bins we recover a $b_\phi(b_1)$ law which is very close to the universality relation (Eq. 5). In fact, we are able to reproduce the results from Adame et al. (2024) with the analysis tools used for this letter.

Another way to verify the tools used here is to select a bin in mass with bias $b_1 \sim 3$, and compare it to one of the bins in $\delta_{h,R}$ with a similar bias value (using all haloes as parent catalogue). This is shown in Fig. A.1, where we observe a very clear PNG effect at low $k$ for the mass bins, whereas we do not observe any PNG response for the density bins.

## Appendix B: Classifying by dark matter overdensity

In the main body, we focused on using biased tracers (haloes or galaxies) for the estimation of local density, $\delta_{t,R}$. This is motivated by assuming this is what we can do with galaxy surveys. One could think of other ways of estimating local density, such as lensing (either from CMB or from galaxy shear), which will be a more direct probe of the matter field, although typically projected to a 2D sky over a long radial kernel.

For this reason, in this appendix we test an ideal scenario where we would have access to the matter field, $\delta_{m,R}$ and we can classify haloes according to this density. From the resulting classification, we can compute the linear ($b_1$) and PNG ($b_\phi$) bias as before, obtaining Fig. B.1. We find that there is a strong deviation from universality, with negative $b_\phi$ for $0.5 < b_1 < 1.5$. Nevertheless, what remains unchanged with respect to other tracers is that for $b_1 = 0$ we still find a clear $b_\phi = 0$.

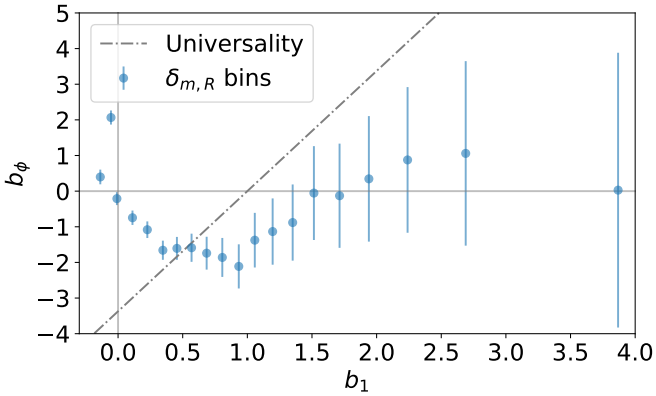


**Fig. B.1.** PNG response $b_\phi$ as a function of linear bias $b_1$ for haloes classified as a function of local matter density $\delta_{m,R}$ using all PNG-UNITsim ($f_{\rm NL} = 100$) haloes above 20 particles.